applied sciences

MDPI

Article

Removal of Lead(II) from Synthetic Wastewater by *Lavandula Pubescens* Decne Biosorbent: Insight into Composition–Adsorption Relationship

Ali Q. Alorabi [1], Fahad A. Alharthi [2,*], Mohamed Azizi [3], Nabil Al-Zaqri [2], Adel El-Marghany [2] and Khaled A. Abdelshafeek [4]

1 Chemistry Department, Faculty of Science, Albaha University, P.O. Box: 1988, Albaha 65779, Saudi Arabia; aalorabi@bu.edu.sa
2 Department of Chemistry, College of Science, King Saud University, Riyadh 11451, Saudi Arabia; nalzaqri@ksu.edu.sa (N.A.-Z.); amarghany@ksu.edu.sa (A.E.-M.)
3 Chemistry Department, Faculty of Science and Arts, Albaha University, Qilwah 65941, Saudi Arabia; mazizi@bu.edu.sa
4 Chemistry Department, Faculty of Science and Arts (Almukhwah), Albaha University, Albaha 65779, Saudi Arabia; kelbarbary@bu.edu.sa
* Correspondence: fharthi@ksu.edu.sa

Received: 23 September 2020; Accepted: 20 October 2020; Published: 24 October 2020

Abstract: In this work, the widely-abundant, cheap, wild plant *Lavandula pubescens* Decne was evaluated as an adsorbent for removing Pb(II) ions from wastewater. The chemical composition of the plant was partially isolated and characterized by the corresponding techniques, including gas chromatography–mass spectrometry, gas liquid chromatography, and FTIR spectroscopy. The adsorption capacity of the dried plant material for Pb(II) ions increased with increasing contact time, initial ion concentration, and temperature, while it decreased with increasing adsorbent dosage. The optimum condition for Pb(II) adsorption was determined as 550 mg/L initial metal concentration, pH ≤ 7, and 90 min of contact. The best fit for Pb(II) adsorption isotherms was the linear form of the Freundlich model; however, the maximum capacity indicated by Langmuir was 91.32 mg/g. The experimental data fit better the pseudo-second-order kinetic model (R^2 = 0.969), suggesting chemisorption process. Thermodynamic data revealed an endothermic, nonspontaneous, and adsorption process favored at higher concentrations.

Keywords: *Lavandula pubescens*; low-cost biosorbent; adsorption; lead ion removal; water treatment; GC-MS analysis

1. Introduction

Heavy metal contamination of water is a growing problem, because of the industrial and technological development and the wide use of the associated materials. Toxic heavy metals released during manufacturing processes pose a serious threat to the environment, due to their non-degradable character and high possibility of bioaccumulation, particularly in plants [1]. The intake and accumulation of heavy metals also have serious health consequences for humans, such as cancer, organ failure, nervous system disorder, growth retardation, etc. [2–4]. The toxicity of lead has been known since antiquity, and remains a problem today [5]. Lead can be found in water, soil, air, in water transport systems due to the corrosion of lead pipes, from industrial discharges, and through the use of leaded gasoline. Therefore, policymakers and researchers are looking for sustainable ways to treat wastewater containing toxic metals released from industrial sources.

Established technologies for removing toxic metals from wastewater include membrane filtration [6], chemical precipitation [7], and ion exchange [8], as well as reverse osmosis and adsorption on activated carbon [9]. However, many of these methods are expensive, have unpredictable performance, and/or generate toxic byproducts that are difficult to manage. Hence, their applications are limited [9]. The adsorption technique is a relatively successful one, since it features a simple design, easy operation, and high separation efficiencies [10,11]. Activated carbon is the most common sorbent for separating heavy metal from wastewater. However, it still suffers from a high cost, problems in regeneration and disposal, and dissolution under extremely acidic conditions. Therefore, there is a growing research effort to find cheaper and greener alternative adsorbents [12–14].

Many researchers have used natural biomaterials, such as agricultural or plant wastes for immobilizing environmental pollutants, because they are inexpensive, renewable, abundant, environmentally friendly, and biodegradable [15]. Example adsorbents for removing toxic metals include vegetable peels, banana peels, coffee grounds, cactus, rice straw, wheat straw, *Diplotaxis harra* (wall rocket), and *Glebionis coronaria* (crown daisy) [9,15–19]. The biosorption processes could occur through different mechanisms (e.g., chemisorption, complexation, adsorption–complexation on surfaces and pores, ion exchange, microprecipitation, and sorption by physical forces). They are also influenced by many parameters modulating the interaction between the adsorbate and absorbent, such as pH, initial metal ion concentration, biomass dosage, temperature, contact time, and the presence of other metal ions in solution [4,15].

Lavandula pubescens (*L. pubescens*) belongs to the genus of lavender (*Lamiaceae* family). It grows abundantly as a shrub in the wild across Saudi Arabia. *L. pubescens* has been predominantly used in aromatherapy as a relaxant and a carminative, antimicrobial, antitumor, and sedative agent, owing to its phytochemical components, such as essential oil, flavonoids, coumarins, polyphenolics, alkaloids, and terpenes [20,21]. To our best knowledge, however, only a few studies have employed this plant material for heavy metal removal [22].

Herein, the dried aerial part of *L. pubescens* was used for the first time as adsorbent without any physical or chemical pretreatment for removing Pb(II) ions from water. This method does not require any toxic and costly material or complicated procedure. To gain better insight into the plant constituents–adsorption activity relationship, before the adsorption experiments, the plant was first characterized by gas chromatography–mass spectrometry (GC/MS), gas liquid chromatography (GLC), and Fourier transform infrared (FTIR) spectroscopy. Therefore, the following influencing parameters for adsorption were considered: the contact time, initial concentration of Pb(II) ions, adsorbent dosage, pH, and temperature. The sorption equilibrium isotherms and kinetic data were also studied using different models.

2. Materials and Methods

2.1. Materials

2.1.1. Chemicals

Lead nitrate ($Pb(NO_3)_2$, 99%), sodium hydroxide pellets (NaOH, 98%), potassium hydroxide pellets (KOH, 85%), and nitric acid (HNO_3, 65%) were purchased from Alfa Aesar, Karlsruhe, Germany. Ethanol (EtOH, 96%), methanol (MeOH, 99.8%), hydrochloric acid (HCl, 36%), and sodium sulfate anhydrous (Na_2SO_4) were procured from Fisher Chemical, Loughborough, UK. All chemicals were used as received without further treatments, unless otherwise stated.

2.1.2. Biomass

The aerial parts (stems and leaves) of *L. pubescens Decne* (LPD) plant were collected from the Albaha region in western Saudi Arabia during April 2018. The biomass was washed thoroughly with distilled water to remove external dirt and, subsequently, air-dried at room temperature until constant

weight was reached. The dried material was ground using an electric grinder to obtain fine powder. This as-prepared material was then stored in a plastic bottle for further use in the solvent-extraction and adsorption experiments.

2.1.3. Adsorbate

A stock solution of Pb(II) (1000 mg/L) was prepared in distilled water. The working solutions were obtained by dilution and, when needed, the pH of the desired working solutions was adjusted using 0.1 M of either NaOH or HNO_3. The pH value was monitored by a Benchtop Orion 3 Star pH-meter (Thermo Scientific, Beverly, MA, USA), previously calibrated with standard buffers. A standard curve of the lead(II) ions was established in the range 2–10 ppm. The sample concentrations were analyzed using flam atomic absorption spectroscopy (FAAS) (PinAAcle 900T, PerkinElmer, Waltham, MA, USA) with a deuterium lamp (BGC-D2) and air-acetylene flame. Accordingly, concentrations were calculated via Beer–Lambert law, with reference to the standard curve.

2.2. Extraction of L. Pubescens Constituents

The plant powder (200 g) was defatted with petroleum ether at 40–60 °C using a Soxhlet apparatus. To remove the pigments, the petroleum ether extract was passed through fuller's earth, filtered, dehydrated over anhydrous sodium sulfate, and dried at 30 °C under reduced pressure, using a rotary evaporator to give a pale yellow residue (3.8 g). Subsequently, the residue was dissolved in hot acetone (300 mL) and left to settle down overnight at room temperature. The obtained precipitate was filtered, washed with cold acetone, and recrystallized from chloroform/methanol to finally afford 0.75 g white crystals, the precipitate (acetone insoluble fraction, AIF) representing the mixture of fatty alcohols and hydrocarbons. The filtrate, acetone soluble fraction (ASF) was evaporated till dryness (2.5 g residue) and subjected to saponification with KOH/MeOH to afford an unsaponifiable fraction (USF) and total fatty acids fraction (FAF). The FAF was methylated with MeOH/HCl to afford fatty acid methyl esters (FAME).

Alcoholic extract was obtained using aqueous methanol 90%. Hence, 20 g of the dried powdered plant was macerated, sequentially, three times, each with 100 mL MeOH. The combined methanolic extract was evaporated *in vacuo* till dryness before FTIR analysis. The constituents of the lipid fractions (AIF, USF, and FAME) were identified by gas chromatography coupled mass spectrometry (GC/MS) and/or gas liquid chromatography (GLC), using the conditions described below.

2.3. Identification of the Isolated Chemical Constituents

2.3.1. GC/MS Analysis of AIF

The GC/MS analysis was carried out using a TRACE GC Ultra gas chromatograph from Thermo Scientific (Thermo Fisher Scientific Inc., Waltham, MA, USA), coupled with a Thermo-MS detector (ISQ Single Quadrupole Mass Spectrometer). The GC/MS system was equipped with a TG-5MS column (30 m × 0.25 mm i.d., 0.25 µm film thickness). Helium carrier gas was employed at a flow rate of 1.0 mL/min and a split ratio of 1:10. The temperature program was 60 °C for 1 min, rising at 3.0 °C/min to 240 °C, and held for 1 min. The injector and detector were held at 240 °C. The sample was diluted at 1:10 (*v*/*v*) in hexane, and 0.2 µL of the mixture was injected each time. Mass spectra were obtained by electron ionization (EI) at 70 eV in the *m*/*z* range of 40–450. Most of the compounds were identified based on the authentic chemicals, Wiley Spectral Library collection, and National Institute of Standards and Technology (NIST) library.

2.3.2. GLC Analysis of AIF and FAME

The GLC analyses were performed on a Varian model 3700 GC instrument (Varian Inc., Palo Alto, CA, USA) equipped with a capillary column (AG-Bp-70, poly silphenylenesiloxane, 60 m length, 320 µm internal diameter, 0.25 µm film thickness). For the AIF, the following temperature program

was used: starting 70 °C and rising at 4 °C/min to 270 °C. The injector and detector were held at 280 °C and 290 °C, respectively. For FAME, the temperature program was 70 °C and rising at 4 °C/min to 190 °C; and the injector and detector were held at 240 °C and 280 °C, respectively. The flow rates of N_2 and H_2 were 30 mL/min, and that of air was 300 mL/min.

2.4. FTIR Analysis

Fourier transform infrared (FTIR) analysis of the as-prepared plant powder adsorbent and ethanolic extract were performed to identify the essential functional groups predominantly responsible for the material adsorption activity. The measurement was carried out using a Nicolet iS50 FTIR spectrophotometer (Thermo Scientific) equipped with an attenuated total reflection (ART) accessory, over the range 4000–650 cm^{-1}, with a resolution of 4 cm^{-1} and total cycles of 32.

2.5. Adsorption Studies

2.5.1. Batch Adsorption Experiments

The adsorption equilibrium of lead ion with LPD adsorbent was carried out in 50-mL Eppendorf tubes; agitated at 150 rpm, and at the suitable conditions. Thus, the following parameters were optimized: initial lead(II) ion concentration (10–550 ppm), adsorbent dosages (0.1–2 g), pH value of the solution (3–7), and temperature (30–50 °C). For the kinetic adsorption study, the tubes were shaken for 0, 20, 30, 60, 90, 120, and 180 min under the following conditions (2 × 7 tubes): LPD dose 0.2 g, Pb^{2+} adsorption solution 50 mL, Pb^{2+} concentration 55 ppm, pH 6, temperature 25 °C, and agitation 150 rpm. After each experiment, the adsorbent LPD was removed by filtration (Whatman filter paper, No. 1) and the residual ion concentration in the filtrate was measured using FAAS. All the experiments were performed in duplicate and averaged.

2.5.2. Adsorption Modelling

The percentage of metal ion removal (Re, %) and the equilibrium adsorption capacity (q_e, mg/g) were computed using the following equations:

$$R_e\% = \left(\frac{C_0 - C_e}{C_0}\right) \times 100 \quad (1)$$

$$q_e = \frac{(C_0 - C_e)\ V}{m} \quad (2)$$

where C_0 and C_e (mg/L) are respectively the initial and equilibrium metal concentrations, V (L) is the volume of the metal solution, and m (g) is the mass of adsorbent used.

Adsorption isotherm was evaluated using Langmuir and Freundlich adsorption models [23]. The Langmuir model generally assumes monolayer adsorption, whereas Freundlich suggests a heterogeneous surface with an exponential distribution of active sites and their energies. The linear forms of the two isotherms can be expressed by Equations (3) and (4) [23].

$$\frac{C_e}{q_e} = \frac{1}{K_L q_m} + \frac{C_e}{q_m} \quad (3)$$

$$lnq_e = lnK_F + (lnC_e)/n \quad (4)$$

where C_e, q_e, and q_m (mg/g) have the same meaning as above, K_L (L/mg) is the Langmuir constant, describing the adsorption affinity for the adsorbent, K_F (mg/g) is the Freundlich coefficient, reflecting the adsorption capacity, and $1/n$ is the adsorption intensity, with the n value describing whether the adsorption is a physical ($n < 1$) or chemical ($n > 1$) process. If $n = 1$, then the adsorption is linear.

To evaluate the adsorption kinetic, the pseudo-first-order (PFO) and pseudo-second-order (PSO) models were used as described, respectively, by Lagergren–Svenska and Ho–McKay [23,24]. The linear form of Lagergren first-order rate equation is:

$$log(q_e - q_t) = log(q_e) - \frac{k_1 t}{2.303} \quad (5)$$

where q_e and q_t (mg/g) are, respectively, the adsorption capacity of metal ion at equilibrium and after time t (min), and k_1 (1/min) is the PFO rate constant.

The linear form of the second-order rate equation is:

$$\frac{t}{q_t} = \frac{1}{k_2\, q_e^2} + \frac{t}{q_e} \quad (6)$$

where k_2 is the PSO equilibrium constant (mg/(g·min)).

Adsorption thermodynamic parameters, including Gibbs free energy (ΔG°), enthalpy (ΔH°), and entropy (ΔS°) were calculated using the van't Hoff model, Equations (7)–(9).

$$\Delta G^\circ = -RTlnK_s \quad (7)$$

$$lnK_s = -\frac{\Delta H^\circ}{RT} + \frac{\Delta S^\circ}{R} \quad (8)$$

where

$$K_s = \frac{q_e}{C_e} \quad (9)$$

where K_s (L/g) is the apparent equilibrium constant, R (8.314 J/(mol·K)) is the universal gas constant, T (K) is the adsorption temperature; all the other parameters reflect the same meaning as described in the isotherms above.

3. Results and Discussion

3.1. Chemical Constituents in the Lipid Fraction

The lipid constituents in the plant were extracted with petroleum ether and fractionated to acetone insoluble fraction (AIF), unsaponifiable constituents (USF), and fatty acids. The AIF was analyzed by GC/MS (Table 1) and found to contain at least 10 hydrocarbons, of which the main compounds were *n*-octacosane ($C_{28}H_{58}$, 30.34%) and hexatriacontane ($C_{36}H_{74}$, 27.50%). The USF was analyzed with GLC, and the data are summarized in Table 2. This fraction contained *n*-hydrocarbons, triterpenes, and sterols. The hydrocarbon fraction accounted for about 93.05% of the weight, and included 16 identified components, with docosane ($C_{22}H_{46}$) being the major one (23.54%). The triterpene fraction contained only one compound, which was identified as amyrine. The sterol fraction was composed of three compounds (cholesterol, stigmasterol, and sitosterol), with stigmasterol as a principal component (3.4%).

Table 1. GC/MS data of acetone insoluble fraction of *L. pubescens* Decne extract.

Peak No.	R_t (min)	Rel. %	Formula	Mol. wt.	Compounds
1	42.41	2.37	$C_{22}H_{46}$	310	*n*-Docosane
2	48.76	3.06	$C_{23}H_{48}$	324	*n*-Tricosane
3	51.13	6.56	$C_{27}H_{56}$	380	*n*-Heptacosane
4	52.40	30.43	$C_{28}H_{58}$	394	*n*-Octacosane
5	54.14	2.15	$C_{29}H_{60}$	408	*n*-Nonacosane
6	54.42	7.62	$C_{29}H_{60}$	408	2-Methyloctacosane
7	55.13	5.63	$C_{30}H_{62}$	422	*n*-Triacontane
8	56.56	9.72	$C_{35}H_{72}$	492	*n*-Pentatriacontane
9	57.41	27.86	$C_{36}H_{74}$	506	*n*-Hexatriacontane
10	62.7	4.60	$C_{44}H_{90}$	618	*n*-Tetratetracontane

R_t is the retention time and Rel.% is the relative percentage in the chromatogram.

Table 2. GLC data of USF of *Lavandula pubescens* Decne (LPD).

Peak No.	R_t (min)	Rel. %	Chemical Formula	Compounds
1	7.74	3.85	$C_{13}H_{28}$	Tridecane
2	11.35	1.98	$C_{16}H_{34}$	Hexadecane
3	12.74	3.07	$C_{17}H_{36}$	Heptadecane
4	14.22	8.08	$C_{18}H_{38}$	Octadecane
5	15.65	10.01	$C_{19}H_{40}$	Nonadecane
6	16.55	8.25	$C_{20}H_{42}$	Eicosane
7	18.33	8.26	$C_{21}H_{44}$	Heneicosane
8	19.48	23.54	$C_{22}H_{46}$	Docosane
9	21.021	5.97	$C_{23}H_{48}$	Tricosane
10	22.319	2.55	$C_{24}H_{50}$	Tetracosane
11	22.964	4.04	$C_{25}H_{52}$	Pentacosane
12	24.680	2.24	$C_{26}H_{54}$	Hexacosane
13	25.258	5.92	$C_{27}H_{56}$	Heptacosane
14	26.433	2.71	$C_{28}H_{58}$	Octacosane
15	26.965	1,84	$C_{29}H_{60}$	Nonacosane
16	27.674	1.09	$C_{30}H_{62}$	Triacontane
17	30.369	0.96	$C_{27}H_{46}O$	Cholesterol
18	31.132	3.40	$C_{29}H_{48}O$	Stigmasterol
19	32.468	1.54	$C_{29}H_{50}O$	β-Sitosterol
20	35.062	1.05	$C_{30}H_{50}O$	α-Amyrine

The fatty acids mixture (Table 3) was found to contain eight acids: four saturated ones (59.48%) with palmitic acid (23.69%) as a main one, and four unsaturated acids (40.54%) with oleic acid as the main one (14.23%). Our results differ from those reported by Gouda et al. and Akhlaghi et al. [25,26]. Those authors analyzed the unsaponifiable matter of *L. pubescens* growing in Egypt, and identified 5-hydroxy1,3,4-trimethoxy-7-methyl-6propar-naphthalene (36.64%) as the major component followed by hentriacontane (8.09%). Regarding fatty acids, oleic acid (12.72%) was the major fatty acid methyl ester, in line with the results of Akhlaghi et al. [26], who identified the main fatty acid methyl esters in the leaf and stem of *Lavandula* officinalis collected from Iran as α-linolenic acid (43.2 and 21.0%, respectively), oleic acid (3.4 and 14.5%), and palmitic acid (7.4 and 12.4%).

Table 3. Gas liquid chromatography (GLC) data of fatty acid methyl esters (FAME) fraction of *L. pubescens* Decne.

Peak No.	R_t (min)	Rel. %	Notation	Compounds
1	21.15	23.69	C16(0)	Palmitic acid
2	25.06	14.51	C18(1)	Oleic acid
3	26.03	8.99	C18(2)	Linoleic acid
4	27.04	13.72	C18(3)	Linolenic acid
5	28.65	11.24	C20(0)	Arachidic acid
6	29.48	3.30	C20(4)	Arachidonic acid
7	30.75	3.24	C22(0)	Behenic acid
8	32.45	21.31	C24(0)	Lignoceric acid

The FTIR spectra of the adsorbent (LPD) and their alcoholic extract are shown in Figure 1. As can be seen, the majority of the functional groups can be identified, allowing the estimation of the adsorption active sites of the biosorbent under investigation. Both spectra exhibited prominent peaks at 3300, 2910, and 1645 cm^{-1}, while peaks at 1400, 1300, 1100, and 1041 cm^{-1} were clearer in the alcoholic extract. However, the reduced intensity of some peaks in the spectra of the LPD, compared to the extract, may be due to the bulky materials, compared to the less complicated contents in the extract. The broad absorption band at 3300 cm^{-1} was assigned to stretching vibrations of hydroxyl functionality in the alcoholic and carboxylic OH groups, while the stretching vibration of (NH) C=O peptide carbonyl groups appeared at 1645 cm^{-1}, with shoulders around 1750 cm^{-1} indicating additional different type of carbonyl groups. Peaks corresponding to the aromatic C=C double bonds could be assigned at 1510 cm^{-1}. The band at 1400 cm^{-1} was due to C–C and C–N stretching, and the peak at 2910 cm^{-1} was assigned to C–H (e.g., methoxy compounds) stretching vibrations. The peak at 1041 cm^{-1} corresponds to C–O stretching vibration of organic compounds, such as ethers, esters, and amides.

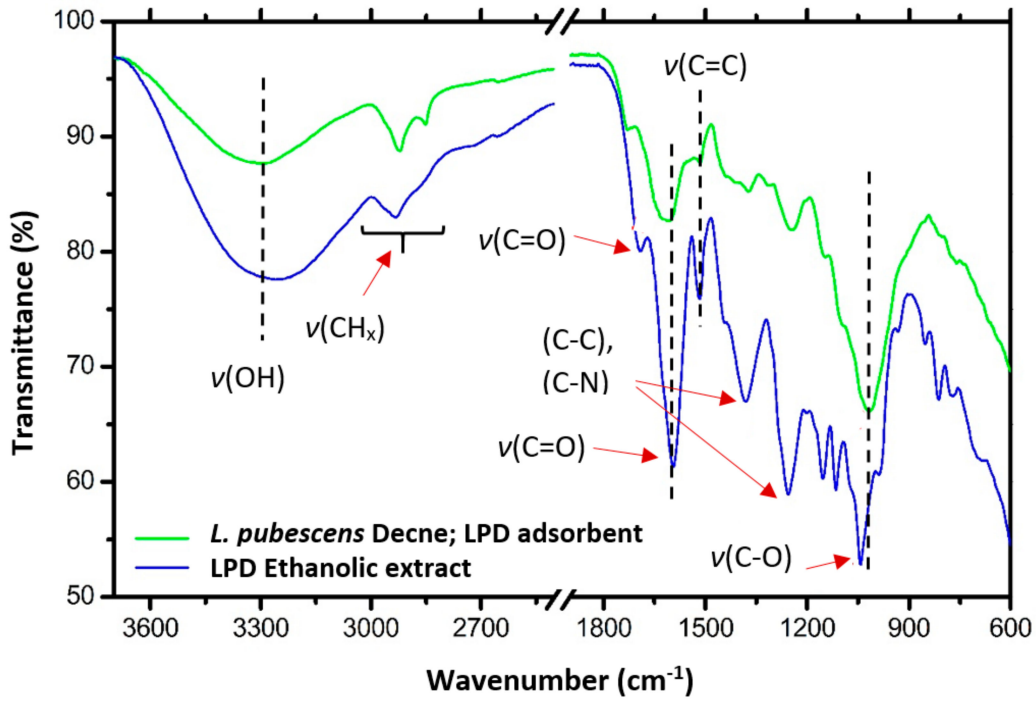

Figure 1. Fourier transform infrared spectra of the adsorbent LPD (green-colored spectra) and the ethanol extract (blue-colored spectra).

Accordingly, in addition to the hydrocarbons, the GC/MS and GLC analysis indicate the presence of adequate amounts of hydroxyl-, carboxyl-, and amide-containing organic compounds such as

sterol, cholesterol, and long-chain saturated and unsaturated fatty acids. These molecules with polar functional groups (OH, COOR, (NH) C=O, and COOH) may play a major role in the interaction with metal ions, providing the adsorbent with the negative charges, and thus increase their adsorption. The FTIR spectra of the dry powder and the extract (Figure 1) clearly showed that hydroxyl, carboxylic, and ester functional groups existed in the plant powder and extract.

3.2. *Adsorption Efficiency of LPD Biomass*

3.2.1. Effect of Contact Time

Figure 2 shows the adsorption profile of Pb^{2+} onto LPD adsorbent over the adsorption period of 0–180 min. It is obvious that, under the applied adsorption conditions, two phases of sorption behavior are present: a relatively fast, initial one from 0 to 90 min, followed by a slow, final phase up to 180 min, the pseudo-equilibrium, with experimental adsorption capacity (q_e) of 4.12 mg/g and removal percentage (R_e) of 32%. The rapid adsorption in the first stage of adsorption can be attributed to the high availability of vacant sites on the adsorbent surface for the heavy metal ions occupation. By reaching the last stage of adsorption, the adsorbed ions cause increased repulsive forces, making the remaining sites difficult to be accessed, resulting in reduced adsorption rate [27]. Similar findings were reported, using banana peels and *Ulva lactuca* for the removal of Pb(II) and Cd(II) [28,29], and *Schoenoplectus californicus* plant for the removal of Cr(III) and Pb(II) [30].

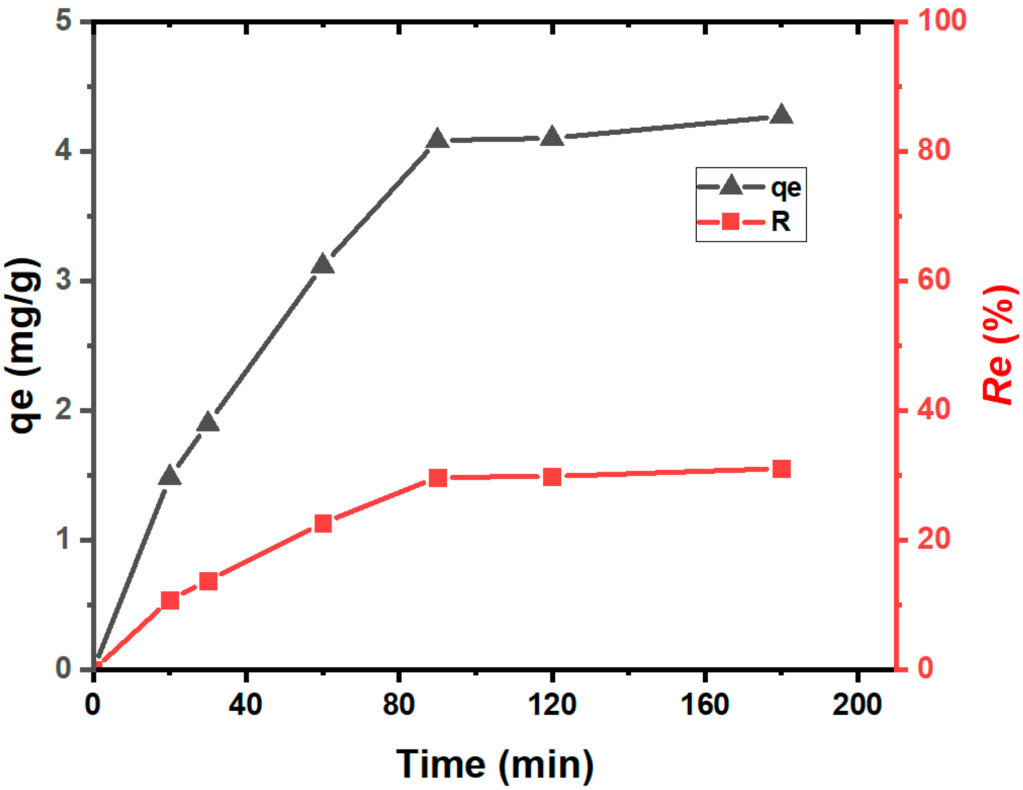

Figure 2. Effect of contact time on the adsorption capacity and removal percentage of lead(II) ions onto LPD. Conditions: 55 ppm Pb^{2+} concentration, 50 mL Pb^{2+} solution volume, 0.2 g LPD adsorbent dose, pH 6, 25 °C adsorption temperature, and 150 rpm agitation speed.

3.2.2. Adsorption Kinetics

The measured adsorption kinetic data were fitted to the linear forms of Lagergren PFO and PSO equations (Equations (5) and (6)). The two models were applied to estimate the adsorption constants (k_1 and k_2) as well as the correlation coefficients (R^2) values for Pb^{2+}. The results are presented in Figure 3

and Table 4. According to the data obtained, the values of q_e (6.91 mg/g) and R^2 (0.969) of the PSO model are more acceptable, describing kinetic behavior with q_e value closer to the experimental one (q_e. Exp.; 4.12 mg/g) compared with that from PFO (15.10 and 0.946, respectively), indicating that the PSO model fits the experimental data better [31]. Therefore, the rate-limiting step of Pb^{2+} adsorption seems to be controlled by a chemical adsorption process via, for example, exchanging of electrons between the adsorbent and adsorbate [32], however, the physical adsorption process cannot be ignored, at least in the last stage of adsorption period. The initial adsorption rate (h; mg/(g·min)) can be calculated from the data of the PSO model, as expressed in Equation (10). However, the calculation indicates low value of h (0.095 mg/(g·min) at the applied adsorption conditions (Table 4).

$$h = k_2 q_e^2 \tag{10}$$

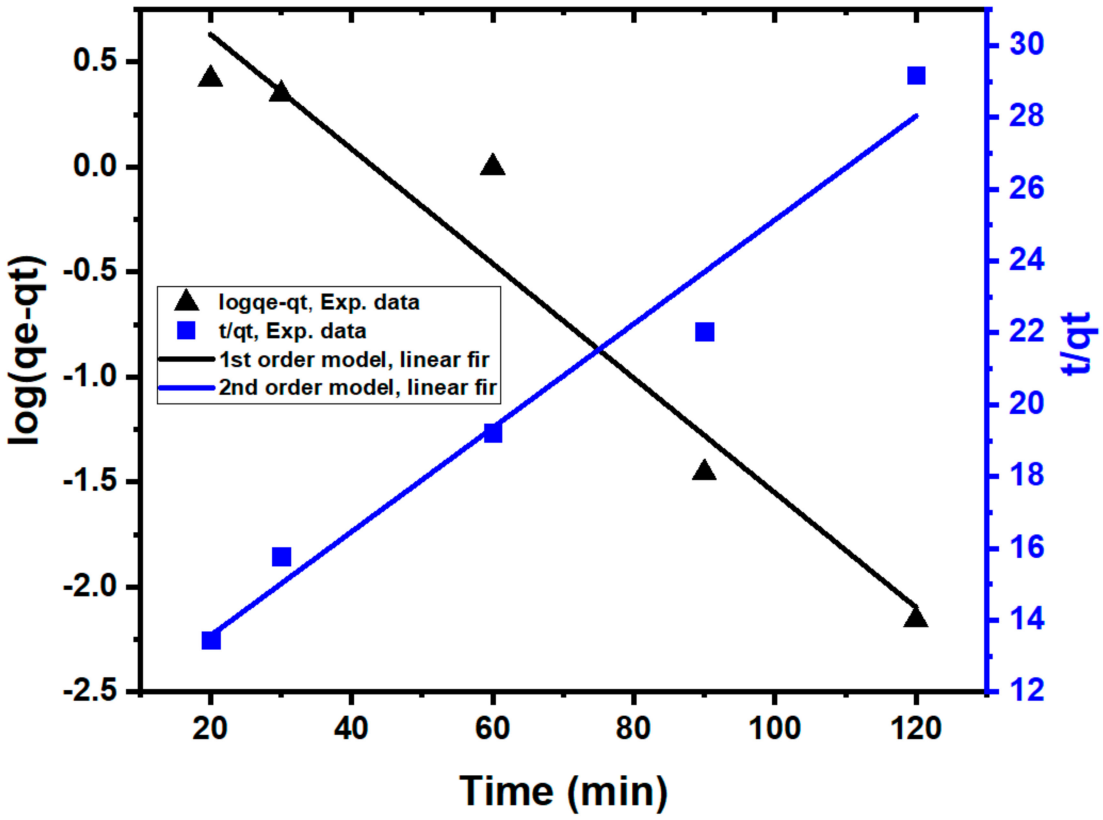

Figure 3. Pseudo-first and pseudo-second order kinetic models for adsorption of Pb^{2+} onto LPD. Conditions: 55 ppm Pb^{2+} initial concentration, 50 mL Pb^{2+} solution volume, 0.2 g LPD adsorbent dose, pH 6, 25 °C adsorption temperature, and 150 rpm agitation speed.

Table 4. Kinetic parameters of pseudo-first and pseudo-second order equations for lead(II) adsorption onto LPD.

q_e. Exp. (mg/g)	Pseudo-First-Order			Pseudo-Second-Order			
	q_e (mg/g)	k_1 (1/min)	R^2	q_e (mg/g)	k_2 (g/(mg·min))	R^2	h (mg/(g·min))
4.12	15.10	0.063	0.946	6.91	0.0020	0.969	0.095

3.2.3. Effect of Solution pH

The pH of solution is a crucial parameter that affects the adsorption process, by influencing both the solubility of the metal ions and the surface characteristics of adsorbent in the aqueous solution [33]. The effect of pH on the biosorption of Pb(II) ions by *L. pubescens* biomass was studied

in the pH range from 3 to 7. In Figure 4a, the maximum adsorption capacity was at pH = 5 (q_e = 12.86 mg/g). However, a slight difference with pH 7 (12.55 mg/g) was observed. At pH lower than 5 (i.e., acidic medium), the additional H^+ compete with the metal cations for active sites on the biomass surface [33], and also repel the metal ions from the surface by electrostatic force. Hence, the adsorption capacity is reduced. In contrast, with pH increase, negatively charged functional groups on the LPD surface (such as carboxyl, phosphate, phosphodiester, sulphonate, and imidazole) attract the positively charged metal ions, and enhance their adsorption [30]. As the pH value increases above 7, however, the OH ions increase in solution and react with the metal ions to form hydroxide precipitates and, therefore, adsorption experiments could not be performed well [34]. From these observations, it can be concluded that the adsorption efficiency of Pb^{2+} ions by *L. pubescens* biomaterial increases as the pH value approaches pH 5. According to literature [29,30], before precipitation occurrence of $Pb(OH)_2$ at pH > 7, the slight decrease in biosorption of lead(II) at pH between 5 and 7 is due to the formation of soluble hydroxide complexes of the lead ions, which compete for the active sites and, as a consequence, decrease the adsorption efficiency. Such competition between biosorption, lead-hydroxyl complexation, and precipitation of the lead ions commonly occurs at pHs close to neutrality (~pH 7) [30]. The chromatography and FTIR analysis indicate that the LPD biosorbent contains dominant organic-based polar or negatively-charged functional groups, such as hydroxyl, carboxyl, ester, amide, and amine; thus, ionic interaction, as one possible adsorption mechanism, with LPD is facilitated by complex formation between metal ions and functional groups on the adsorbent. Moreover, the chemisorption mechanism is supposed to be the dominant mechanism, at least in the first stage of adsorption.

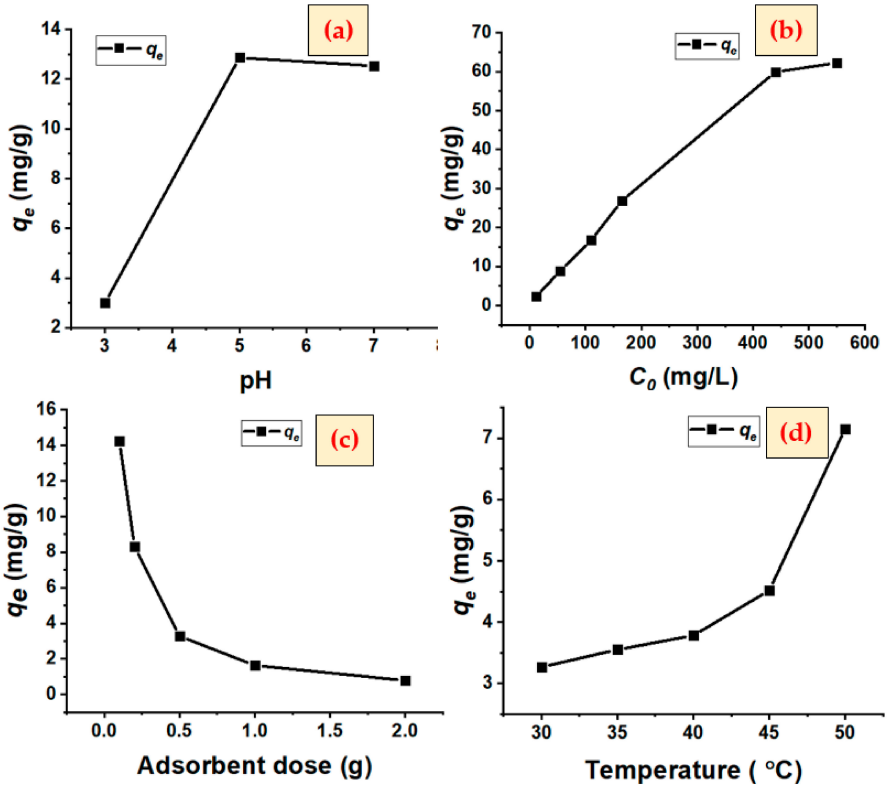

Figure 4. Effect of (**a**) pH value (C_0 = 55 ppm, 0.2 g/50 mL adsorbent dose, temperature = 25 °C, and 150 rpm agitation speed), (**b**) initial lead(II) concentration (0.2 g/50 mL adsorbent dose, pH 6, temperature = 25 °C, and 150 rpm agitation speed), (**c**) adsorbent dosage (C_0 = 55 ppm, 50 mL adsorbent volume, pH 6, temperature = 25 °C, and 150 rpm agitation speed), and (**d**) adsorption temperature (C_0 = 55 ppm, 0.2 g/50 mL adsorbent dose, pH 7, and 150 rpm agitation speed) on the adsorption capacity of *Lavandula pubescens* Decne for removal of lead(II) ions from aqueous media.

3.2.4. Effect of Initial Pb(II) Ion Concentrations

The effects of initial Pb(II) concentrations on the bioadsorption are represented in Figure 4b. When raising the initial Pb(II) ion concentration from 10 to 550 mg/L, and keeping the other parameters constant (0.2 g/50 mL adsorbent dose, pH 6, temperature = 25 °C, and 150 rpm agitation speed), the adsorption capacity increased. This higher metal uptake may be attributed to a higher collision probability of the metal ions with the plant sorbent material. At the highest metal ion concentration (550 mg/L), the adsorption capacity became almost constant, indicating a saturated state due to the limited number of active adsorption sites on the sorbent. The observed result is in line with previous studies using mango kernel [35], *Eichhornia crassipes* [23], and *Oleander* plant [36].

3.2.5. Effect of Adsorbent Dosage

The effect of sorbent dosage on the removal of Pb(II) was also evaluated under the following conditions: 0.1, 0.2, 0.5, 1, and 2 g adsorbent, 50 mL metal ion solution, 55 ppm initial ion concentration, 2 h agitation time, 150 rpm agitation speed, pH ~6, and 25 °C adsorption temperature. From the results in Figure 4c, the highest adsorption capacity (q_e, 14.2 mg/g) of Pb(II) was obtained at 0.1 g (the lowest experimental adsorbent dose); also, with increasing the dose from 0.1 to 0.5 g a noticeable rapid decrease in the adsorbent capacity, to 3.3 mg/g, was observed.. The decreasing behavior of adsorption capacity at higher adsorbent dosage (i.e., above 0.5 g) might be due to aggregation of the adsorption particles, preventing ions reaching the active sites on the adsorbent. However, it can be seen that, when further increasing the adsorption dosage above 0.5 g, the removal percentage of Pb(II) did not change significantly, due to the maximal possible aggregation that may be reached [35]. These findings are consistent with previous studies, in which the dosage is an important factor for effective adsorption [30,35,36]. In reference to the isolated compounds, the chemical composition of the powdered LPD plant may facilitate such aggregation, that is, by physical and hydrogen bonding interaction between, for example, amides, esters, and alcoholic functionalities, meaning that the active site occupation becomes less in the highly compacted bulky materials at higher dose.

3.2.6. Effect of Temperature

The effect of temperature on the adsorption capacity was investigated at 30, 35, 40, 45, and 50 °C, keeping the following parameters constant: adsorbate initial concentrations 55 mg/L, absorbent dosage 0.2 g, adsorption period 2 h, and pH 7. The results depicted in Figure 4d indicate endothermic adsorption mechanism, in which the q_e value increased from 3.2 to 7.15 mg/g when temperature was raised from 30 to 50 °C [37]. Generally, the solution temperature plays a significant role in adsorption by influencing the equilibrium and rate of adsorption processes. Increasing the temperature enhances the diffusion rate of the adsorbate molecules and decreases the solution viscosity; both effects help ions move into adsorbent surfaces and pores of the biosorbent particles, as previously reported for natural plants [38,39] and natural bentonite clay [40]. On the other hand, temperature may facilitate breaking down of the physical and hydrogen bonds, reducing the aggregation events, leading to higher exposure of active sites on the adsorbent for Pb^{2+} ions and, thus, adsorption increase.

3.2.7. Adsorption Isotherms

In order to describe the adsorption equilibrium, the remaining heavy metal ion concentrations (C_e, mg/g) in the solution and the adsorption capacity (q_e, mg/g) were measured and correlated to each other. Langmuir and Freundlich adsorption models (Equations (3) and (4)) were used to fit the isotherm data obtained at different initial ion concentrations (Section 3.2.4) [23,36]. The analysis results are shown in Figure 5a,b, while the fitted parameters are listed in Table 5. According to the results, the Freundlich isotherm fits the data better than the Langmuir model, with correlation coefficient (R^2) values of 0.989 and 0.884, respectively. The maximum adsorption capacity, q_m, calculated from Langmuir isotherm (K_L 0.0074 L/mg), corresponding to the monolayer coverage, was 91.32 mg/g, however,

the K_F value indicates higher affinity for Pb^{2+} adsorption, compared to K_L. The equilibrium factor R_L (dimensionless), Equation (11), is one essential feature of the Langmuir equation, describing the adsorption shape and, therefore, the degree to which the adsorption process is favored: $R_L > 1$, unfavorable monolayer process; $R_L = 1$, linear; $0 < R_L < 1$, favorable; and $R_L = 0$, irreversible [41].

$$R_L = \frac{1}{1 + K_L C_0} \tag{11}$$

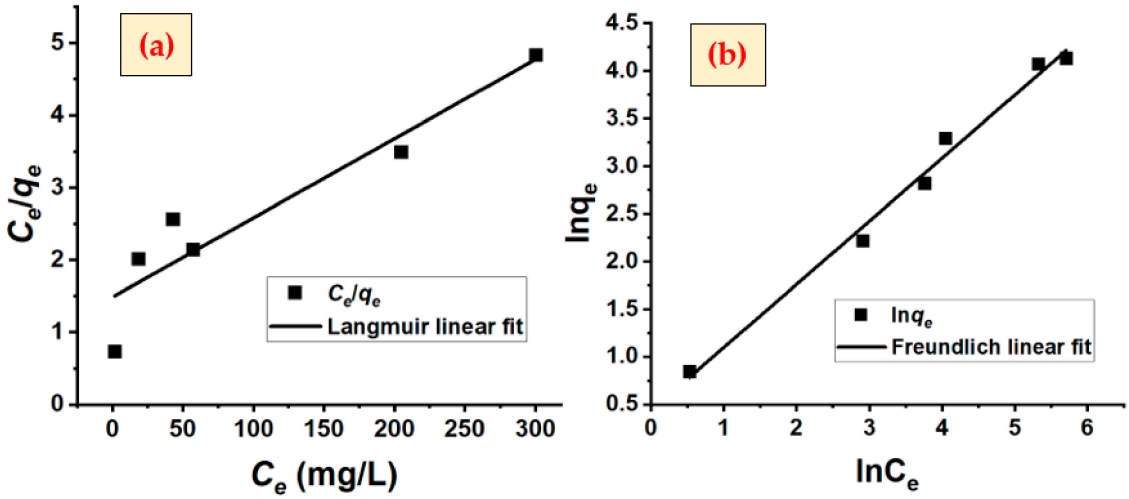

Figure 5. Linearized Langmuir (**a**) and Freundlich (**b**) isotherm equations. Conditions: 10–550 ppm Pb^{2+} concentration, 50 mL Pb^{2+} solution volume, 0.2 g LPD adsorbent dose, pH 6, 25 °C adsorption temperature, and 150 rpm agitation speed.

Table 5. Parameters obtained from Langmuir and Freundlich isotherm models for adsorption of Pb^{2+} ion onto LPD.

Adsorbent	Langmuir				Freundlich			
LPD	q_m (mg/g)	K_L (L/mg)	R^2	R_L (at C_0 (mg/g) = 165, 550)	K_F	1/n	n	R^2
	91.32	0.0074	0.884	0.450, 0.024	2.722	0.662	1.511	0.989

The obtained R_L values (Table 5) are between zero and the unity, thus indicating a favorable adsorption process. The Freundlich model is also characterized by the heterogeneity factor, 1/n, with value of 0.662 indicating good adsorption of Pb^{2+} ions by the adsorbent LPD. Generally, the adsorption is a more suitable fit to Freundlich, and both the separation factor (R_L) and the heterogeneity factor (1/n) indicate a favorable adsorption process on a heterogeneous surface with a tendency toward chemisorption mechanism.

3.2.8. Adsorption Thermodynamics

The thermodynamic parameters, including $\Delta G°$, $\Delta H°$, and $\Delta S°$, can be obtained from the van't Hoff equation, Equation (8), as shown in Figure 6 and Table 6. The positive values of the three parameters indicate an endothermic and nonspontaneous process. However, the adsorption system is greatly dependent on adsorption temperature, becoming spontaneous at high temperature where $T\Delta S$ outweighs ΔH. The positive value of $\Delta S°$ also suggests an increase in the randomness at the solid–liquid interface during the adsorption.

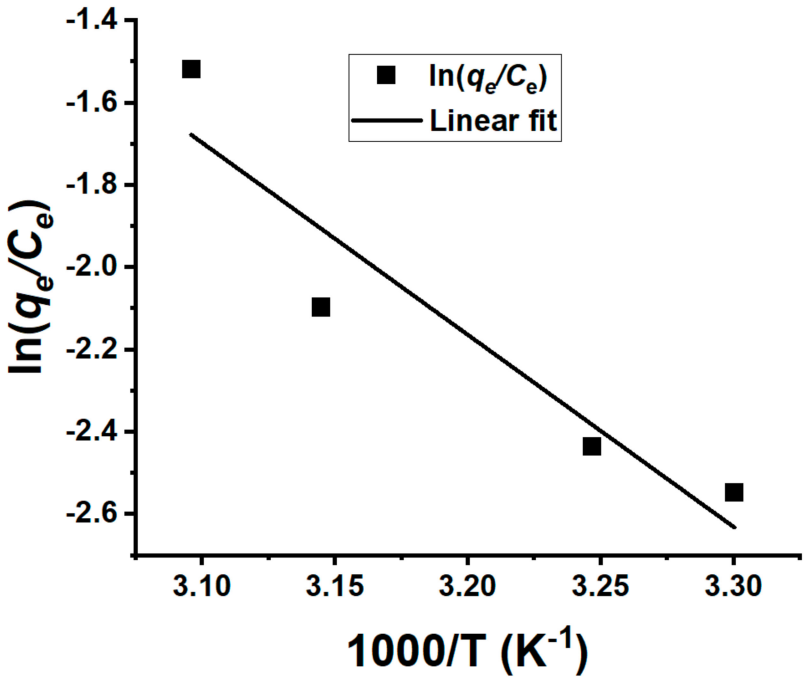

Figure 6. Van't Hoff plot for the adsorption of Pb^{2+} onto *Lavandula pubescens* Decne adsorbent.

Table 6. Thermodynamic parameters for lead(II) ion adsorption onto LPD adsorbent.

T (K)	lnK_s	$\Delta G°$ (kJ/mol)	$\Delta H°$ (kJ/mol)	$\Delta S°$ (J/mol·K)	R^2
303	−2.547	6.417	38.814	106.211	0.8871
308	−2.437	6.239			
318	−2.097	5.545			
323	−1.519	4.079			

Based on the discussed overall results, the adsorption mechanism is an endothermic, PSO, chemical process governed by the Freundlich heterogeneous surface, and is more favorable at high temperature.

Lavandula pubescens is abundantly available in Saudi Arabia, particularly in the western region, and can be collected for free as a raw, low-cost material for, e.g., medical, pharmaceutical, and environmental applications [20,21]. However, as *Lavandula pubescens* biomass used in this work is an abundant wild plant, it can be assumed as a low-cost material, and recovery of the spent adsorbent may be costlier, compared to the raw material itself; therefore, reusability experiments were not further pursued.

3.3. Relative Performance of LPD Biosorbent

A comparison of the adsorption performance of LPD biomass in removal of lead ion from contaminated water with those of various biosorbents reported in literature is shown in Table 7. For simplicity of comparison, the maximum adsorption capacity (q_m) of the biosorbents, as well as the corresponding adsorption conditions, were tabulated. As can be seen, the predicted q_m value of LPD is relatively higher than most of the listed values. It is worth mentioning that, despite no modifications having been carried out on the LPD surface characteristic, its potential for removal of lead(II) is noticeable, and modification may further enhance its adsorption capacity [29]. Adsorption enhancement of modified biosorbent is proven by the work of Calero et al. [42], in which the obtained q_m values of untreated-, H_2SO_4-, HNO_3-, and NaOH-oil tree pruning biosorbents were

27.05, 65.62, 85.09, and 121.60 mg/g, respectively. The difference in the adsorption capacities of various biomasses is attributed to the variety in the chemical and textural properties, including their functional groups' type and abundance. Adsorption conditions are also one important influencer in the adsorption performance of the adsorbent, therefore, optimization of the adsorption parameters may enhance the adsorption efficiency.

Table 7. Comparison of biosorption capacity of various biosorbents for lead(II) ions from aqueous solution.

Biosorbent	q_m (mg/g)	Adsorption Conditions				Reference
		C_0 (mg/L)	pH	T (°C)	Adsorbent Dosage (g/L)	
Schoenoplectus californicus	16.85	2.1–414.4	5	25 ± 1	5	[30]
Banana peels	2.18	30–80	5	25	40	[28]
Ulva lactuca	34.7	10–275	5	20	20	[29]
Moringa oleifera leaves	45.83	80	6	Room T.	1.5	[43]
Solanum melongena leaf	55.55	30–90	5	30	0.4	[44]
Untreated-Olive tree pruning	27.05	40–2400	5	25	10	[42]
H_2SO_4-Olive tree pruning	65.62					
HNO_3-Olive tree pruning	85.09					
NaOH-Olive tree pruning	121.60					
Lavandula pubescens Decne	91.32	10–550	6	25	4	This work

4. Conclusions

In this investigation, the dried aerial parts of a shrub, *L. pubescens*, were tested as a low-cost, abundant, and environmentally-friendly adsorbent for removal of Pb(II) ions from water. The considered variables were: initial metal ion concentrations, solution pH, contact time, temperature, and adsorbent dosage. The adsorption efficiency was correlated to the chemical constituents of *L. pubescens* analyzed by GC/MS and GLC techniques. The result revealed optimal capacity at pH = 5, contact time of 90 min, at low biosorbent dosage, and at higher-temperature and ion initial-concentration. The adsorption isotherms could be better described by the Freundlich model, indicating a multilayer adsorption process. Moreover, the adsorption kinetic obeyed the pseudo-second-order, suggesting a chemisorption process; and evidenced by the thermodynamic data. The adsorption system was found to be endothermic, nonspontaneous, and favored at higher temperature.

Author Contributions: Data curation: F.A.A. and M.A.; formal analysis: M.A.; funding acquisition: F.A.A., A.Q.A., and A.E.-M.; investigation: A.Q.A. and K.A.A.; methodology: F.A.A., N.A.-Z., and A.E.-M.; project administration: A.Q.A.; software: F.A.A.; validation: N.A.-Z.; Writing—Original draft: A.Q.A.; Writing—Review and editing: A.Q.A. All authors have read and agreed to the published version of the manuscript.

Funding: The authors extend their appreciation to the Deanship of Scientific Research at King Saud University for funding this work through the research group No. RGP-1441-305. The authors gratefully acknowledge the financial support by the Deanship of Scientific Research at Albaha University through Project No: 1441/3.

Conflicts of Interest: The authors declare no conflict of interest.

References

1. Ayyappan, R.; Sophia, A.C.; Swaminathan, K.; Sandhya, S. Removal of Pb (II) from aqueous solution using carbon derived from agricultural wastes. *Process. Biochem.* **2005**, *40*, 1293–1299. [CrossRef]
2. Lee, J.-C.; Son, Y.-O.; Pratheeshkumar, P.; Shi, X. Oxidative stress and metal carcinogenesis. *Free Radic. Biol. Med.* **2012**, *53*, 742–757. [CrossRef] [PubMed]
3. Nagajyoti, P.C.; Lee, K.D.; Sreekanth, T. Heavy metals, occurrence and toxicity for plants: A review. *Environ. Chem. Lett.* **2010**, *8*, 199–216. [CrossRef]

4. Afroze, S.; Sen, T.K. A review on heavy metal ions and dye adsorption from water by agricultural solid waste adsorbents. *Water Air Soil Pollut.* **2018**, *229*, 225. [CrossRef]
5. Dridi, C.; Youcef, L. Removal of lead by adsorption on kaolin. *Larhyss J. P-ISSN 1112-3680/E-ISSN 2521–9782* **2016**, *13*, 7–22.
6. Shaalan, H.; Sorour, M.; Tewfik, S. Simulation and optimization of a membrane system for chromium recovery from tanning wastes. *Desalination* **2001**, *141*, 315–324. [CrossRef]
7. Song, S.; Lopez-Valdivieso, A.; Hernandez-Campos, D.; Peng, C.; Monroy-Fernandez, M.; Razo-Soto, I. Arsenic removal from high-arsenic water by enhanced coagulation with ferric ions and coarse calcite. *Water Res.* **2006**, *40*, 364–372. [CrossRef]
8. Alyüz, B.; Veli, S. Kinetics and equilibrium studies for the removal of nickel and zinc from aqueous solutions by ion exchange resins. *J. Hazard. Mater.* **2009**, *167*, 482–488. [CrossRef]
9. Srinivasan, R. *Role of Plant. Biomass in Heavy Metal. Treatment of Contaminated Water*; Anuradha Mishra, J.H.C., Ed.; Royal Society of Chemistry: Cambridge, UK, 2013. [CrossRef]
10. Khan, M.A.; Alqadami, A.A.; Otero, M.; Siddiqui, M.R.; Alothman, Z.A.; Alsohaimi, I.; Rafatullah, M.; Hamedelniel, A.E. Heteroatom-doped magnetic hydrochar to remove post-transition and transition metals from water: Synthesis, characterization, and adsorption studies. *Chemosphere* **2019**, *218*, 1089–1099. [CrossRef]
11. Li, X.; Li, D.; Yan, Z.; Ao, Y. Adsorption of cadmium by live and dead biomass of plant growth-promoting rhizobacteria. *RSC Adv.* **2018**, *8*, 33523–33533. [CrossRef]
12. de Gisi, S.; Lofrano, G.; Grassi, M.; Notarnicola, M. Characteristics and adsorption capacities of low-cost sorbents for wastewater treatment: A review. *Sustain. Mater. Technol.* **2016**, *9*, 10–40. [CrossRef]
13. Jafari-Kang, A.; Baghdadi, M.; Pardakhti, A. Removal of cadmium and lead from aqueous solutions by magnetic acid-treated activated carbon nanocomposite. *Desalin. Water Treat.* **2016**, *57*, 18782–18798. [CrossRef]
14. Huang, C.; Blankenship, D. The removal of mercury (II) from dilute aqueous solution by activated carbon. *Water Res.* **1984**, *18*, 37–46. [CrossRef]
15. Jain, C.K.; Malik, D.S.; Yadav, A.K. Applicability of plant based biosorbents in the removal of heavy metals: A review. *Environ. Process.* **2016**, *3*, 495–523. [CrossRef]
16. Derbe, T.; Batu, H.D.W. Cactus potential in heavy metal (Pb and Cd) removal in water sample collected from rural area around Adigrat town. *Digestion* **2015**, *5*, 11.
17. Dhir, B.; Kumar, R. Adsorption of heavy metals by Salvinia biomass and agricultural residues. *Int. J. Environ. Res.* **2010**, *4*, 427–432. [CrossRef]
18. Hossain, M.; Ngo, H.H.; Guo, W.; Nguyen, T. Removal of copper from water by adsorption onto banana peel as bioadsorbent. *Int. J. Geomate* **2012**, *2*, 227–234. [CrossRef]
19. Seniūnaitė, J.; Vaiškunait, R.; Bolutien, V. Coffee grounds as an adsorbent for copper and lead removal form aqueous solutions. In *Proceedings of The 9th International Conference "Environmental Engineering"*; VGTU Press: Vilnius, Lithuania, 2014. [CrossRef]
20. Minooeianhaghighi, M.; Sepehrian, L.; Shokri, H. Antifungal effects of Lavandula binaludensis and Cuminum cyminum essential oils against Candida albicans strains isolated from patients with recurrent vulvovaginal candidiasis. *J. Mycol. Med.* **2017**, *27*, 65–71. [CrossRef]
21. Al-Badani, R.N.; da Silva, J.K.R.; Mansi, I.; Muharam, B.A.; Setzer, W.N.; Awadh Ali, N.A. Chemical composition and biological activity of Lavandula pubescens essential oil from Yemen. *J. Essent. Oil Bear. Plants* **2017**, *20*, 509–515. [CrossRef]
22. Al-Senani, G.M.; Al-Fawzan, F.F. Study on adsorption of Cu and Ba from aqueous solutions using nanoparticles of Origanum (OR) and Lavandula (LV). *Bioinorg. Chem. Appl.* **2018**, *2018*, 3936178. [CrossRef]
23. Li, Q.; Chen, B.; Lin, P.; Zhou, J.; Zhan, J.; Shen, Q.; Pan, X. Adsorption of heavy metal from aqueous solution by dehydrated root powder of long-root Eichhornia crassipes. *Int. J. Phytoremed.* **2016**, *18*, 103–109. [CrossRef] [PubMed]
24. Ho, Y.-S.; McKay, G. Pseudo-second order model for sorption processes. *Process. Biochem.* **1999**, *34*, 451–465. [CrossRef]
25. Gouda, B.; Mousa, O.; Salama, M.; Kassem, H. Volatiles and lipoidal composition: Antimicrobial activity of flowering aerial parts of Lavandula pubescens Decne. *Int. J. Pharmacogn. Phytochem. Res.* **2017**, *9*. [CrossRef]
26. Akhlaghi, H.; Shafaghat, A.; Salimi, F.; Mohammadhoseini, M. GC-MS analysis of the essential oil from wild Stachys pubescens ten leaves from Northwest Iran. *Anal. Chem. Lett.* **2011**, *1*, 325–327. [CrossRef]

27. Alghamdi, A.A.; Al-Odayni, A.-B.; Saeed, W.S.; Al-Kahtani, A.; Alharthi, F.A.; Aouak, T. Efficient adsorption of lead (II) from aqueous phase solutions using polypyrrole-based activated carbon. *Materials* **2019**, *12*, 2020. [CrossRef]
28. Anwar, J.; Shafique, U.; Salman, M.; Dar, A.; Anwar, S. Removal of Pb (II) and Cd (II) from water by adsorption on peels of banana. *Bioresour. Technol.* **2010**, *101*, 1752–1755. [CrossRef]
29. Sarı, A.; Tuzen, M. Biosorption of Pb (II) and Cd (II) from aqueous solution using green alga (Ulva lactuca) biomass. *J. Hazard. Mater.* **2008**, *152*, 302–308. [CrossRef]
30. Rearte, T.A.; Bozzano, P.B.; Andrade, M.L.; Fabrizio de Iorio, A. Biosorption of Cr (III) and Pb (II) by Schoenoplectus californicus and Insights into the Binding Mechanism. *ISRN Chem. Eng.* **2013**, *2013*, 851602. [CrossRef]
31. Ibrahim, W.M. Biosorption of heavy metal ions from aqueous solution by red macroalgae. *J. Hazard. Mater.* **2011**, *192*, 1827–1835. [CrossRef]
32. Li, Y.; Du, Q.; Wang, X.; Zhang, P.; Wang, D.; Wang, Z.; Xia, Y. Removal of lead from aqueous solution by activated carbon prepared from Enteromorpha prolifera by zinc chloride activation. *J. Hazard. Mater.* **2010**, *183*, 583–589. [CrossRef]
33. Mohammod, M.; Sen, T.K.; Maitra, S.; Dutta, B.K. Removal of Zn 2+ from aqueous solution using castor seed hull. *Water Air Soil Pollut.* **2011**, *215*, 609–620. [CrossRef]
34. FENG, N.-C.; GUO, X.-Y. Characterization of adsorptive capacity and mechanisms on adsorption of copper, lead and zinc by modified orange peel. *Trans. Nonferrous Met. Soc. China* **2012**, *22*, 1224–1231. [CrossRef]
35. Akram, M.; Bhatti, H.N.; Iqbal, M.; Noreen, S.; Sadaf, S. Biocomposite efficiency for Cr (VI) adsorption: Kinetic, equilibrium and thermodynamics studies. *J. Environ. Chem. Eng.* **2017**, *5*, 400–411. [CrossRef]
36. Abu-El-Halawa, R.; Zabin, S.; Abu-Sittah, H. Investigation of methylene blue dye adsorption from polluted water using oleander plant (Al defla) tissues as sorbent. *Am. J. Environ. Sci.* **2016**, *12*, 213–224. [CrossRef]
37. Saha, R.; Mukherjee, K.; Saha, I.; Ghosh, A.; Ghosh, S.K.; Saha, B. Removal of hexavalent chromium from water by adsorption on mosambi (Citrus limetta) peel. *Res. Chem. Intermed.* **2013**, *39*, 2245–2257. [CrossRef]
38. Barka, N.; Abdennouri, M.; el Makhfouk, M.; Qourzal, S. Biosorption characteristics of cadmium and lead onto eco-friendly dried cactus (Opuntia ficus indica) cladodes. *J. Environ. Chem. Eng.* **2013**, *1*, 144–149. [CrossRef]
39. Afroze, S.; Sen, T.K.; Ang, H.M. Adsorption removal of zinc (II) from aqueous phase by raw and base modified Eucalyptus sheathiana bark: Kinetics, mechanism and equilibrium study. *Process. Saf. Environ. Prot.* **2016**, *102*, 336–352. [CrossRef]
40. Sen, T.K.; Gomez, D. Adsorption of zinc (Zn^{2+}) from aqueous solution on natural bentonite. *Desalination* **2011**, *267*, 286–294. [CrossRef]
41. Alghamdi, A.A.; Al-Odayni, A.-B.; Saeed, W.S.; Almutairi, M.S.; Alharthi, F.A.; Aouak, T.; Al-Kahtani, A. Adsorption of Azo Dye Methyl orange from aqueous solutions using alkali-activated polypyrrole-based graphene oxide. *Molecules* **2019**, *24*, 3685. [CrossRef] [PubMed]
42. Calero, M.; Pérez, A.; Blázquez, G.; Ronda, A.; Martín-Lara, M.A. Characterization of chemically modified biosorbents from olive tree pruning for the biosorption of lead. *Ecol. Eng.* **2013**, *58*, 344–354. [CrossRef]
43. Imran, M.; Anwar, K.; Akram, M.; Shah, G.M.; Ahmad, I.; Samad Shah, N.; Khan, Z.U.H.; Rashid, M.I.; Akhtar, M.N.; Ahmad, S. Biosorption of Pb (II) from contaminated water onto Moringa oleifera biomass: Kinetics and equilibrium studies. *Int. J. Phytoremed.* **2019**, *21*, 777–789. [CrossRef] [PubMed]
44. Yuvaraja, G.; Krishnaiah, N.; Subbaiah, M.V.; Krishnaiah, A. Biosorption of Pb (II) from aqueous solution by Solanum melongena leaf powder as a low-cost biosorbent prepared from agricultural waste. *Colloids Surf. B* **2014**, *114*, 75–81. [CrossRef] [PubMed]

Publisher's Note: MDPI stays neutral with regard to jurisdictional claims in published maps and institutional affiliations.

© 2020 by the authors. Licensee MDPI, Basel, Switzerland. This article is an open access article distributed under the terms and conditions of the Creative Commons Attribution (CC BY) license (http://creativecommons.org/licenses/by/4.0/).